A Combined Fuzzy Pixel-Based and Object-Based Approach for Classification of High-Resolution Multispectral Data Over Urban Areas

Aaron K. Shackelford, *Student Member, IEEE* and Curt H. Davis, *Senior Member, IEEE*

***Abstract*—In this paper, we present an object-based approach for urban land cover classification from high-resolution multispectral image data that builds upon a pixel-based fuzzy classification approach. This combined pixel/object approach is demonstrated using pan-sharpened multispectral IKONOS imagery from dense urban areas. The fuzzy pixel-based classifier utilizes both spectral and spatial information to discriminate between spectrally similar *Road* and *Building* urban land cover classes. After the pixel-based classification, a technique that utilizes both spectral and spatial heterogeneity is used to segment the image to facilitate further object-based classification. An object-based fuzzy logic classifier is then implemented to improve upon the pixel-based classification by identifying one additional class in dense urban areas: nonroad, nonbuilding impervious surface. With the fuzzy pixel-based classification as input, the object-based classifier then uses shape, spectral, and neighborhood features to determine the final classification of the segmented image. Using these techniques, the object-based classifier is able to identify *Buildings*, *Impervious Surface*, and *Roads* in dense urban areas with 76%, 81%, and 99% classification accuracies, respectively.**

***Index Terms*— Fuzzy logic, high-resolution imagery, image processing, urban land cover.**

I. Introduction

With the recent availability of commercial high-resolution remote sensing multispectral imagery from sensors such as IKONOS and QuickBird, it is possible to identify small-scale features such as individual roads and buildings in urban environments. Road network and building footprint identification are important tasks for many applications. For example, The National Map [1] being developed by the U.S. Geological Survey (USGS) will provide accurate, current, and nationally consistent digital data for the United States and its territories. The National Map will contain high-resolution orthorectified digital imagery, surface elevation data, several vector feature data layers, geographic names for physical and cultural features, and land cover classification maps. Included in the vector data are feature layers for both the road network and the building footprints. Potential uses for the image and feature data include urban growth planning, emergency response and management, and homeland security applications. The vision for The National Map includes near-real-time adaptation of the map to changes. Thus, automated and semiautomated methods for the classification of roads, buildings, and other land cover types in the urban environment are of great interest.

Automated and semiautomated land-cover classification and road/building extraction can be accomplished using either pixel-based or object-based approaches. Pixel-based classification schemes seek to identify the class of each pixel in the imagery by comparing the n-dimensional data vector for each pixel with the prototype vector for each class. The data vectors typically consist of a pixel's gray-level values from multispectral channels and/or textural and contextual measures that have been computed from those channels. Textural and contextual measures contain information about the spatial distribution of tonal variations within a band. Object-based approaches do not operate directly on individual pixels but on objects consisting of many pixels that have been grouped together in a meaningful way by image segmentation. In addition to spectral and textural information utilized in pixel-based classification methods, image objects also allow shape characteristics and neighborhood relationships to be used for the object's classification. However, the success of object-based classification approaches is very dependent on the quality of the image segmentation.

Because of the complex nature and diverse composition of land cover types found within the urban environment, the production of accurate urban land cover maps from high-resolution satellite imagery is a difficult task. Conventional methods for pixel-based classification of multispectral remote sensing imagery [2] such as parallelepiped, minimum distance from means, and maximum likelihood only utilize spectral information and consequently have limited success in classifying high-resolution urban multispectral images [3]. As many urban land cover types, such as roads, buildings, parking lots, etc., are spectrally similar, spatial information such as texture and context must be exploited to produce more accurate classification maps [4]. In addition to the spectral similarity between land cover types, remote sensing images contain mixed pixels, making it difficult to classify a pixel as belonging to only one class. Fuzzy classification techniques allow pixels to have membership in more than one class and therefore better represent the imprecise nature of the data [5], [6]. For several examples of pixel-based techniques for urban land cover classification and/or road and building extraction we refer the reader to [7]–[11].

Manuscript received September 30, 2002; revised June 8, 2003. The work of A. K. Shackelford was supported by the National Aeronautics and Space Administration (NASA) under Graduate Student Research Program Grant NASA/GSRP NGT13-52747. The work of C. H. Davis was supported by the Raytheon Synergy program under Subcontract 012100MJ-3 from NASA.

The authors are with the Department of Electrical and Computer Engineering, University of Missouri, Columbia, MO 65211 USA (e-mail: DavisCH@missouri.edu).

Digital Object Identifier 10.1109/TGRS.2003.815972

A variety of segmentation techniques have been applied to remote sensing imagery with varying degrees of success. Segmentation of remotely sensed images is a difficult problem due to mixed pixels, spectral similarity, and the textured appearance of many land-cover types. Many segmentation algorithms are based on a region-growing approach where pixels are iteratively grouped into regions based on predefined similarity criteria. Examples of region-growing approaches can be found in [12]–[14]. Pixel classification and region growing were combined in [15] for image segmentation and classification. A segmentation and classification approach using a Markov random field model is presented in [16]. A segmentation method for high-resolution satellite imagery using residuals of morphological opening and closing transforms is presented in [17], and a neural-network-based approach for classifying urban areas using this morphological segmentation is given in [18]. An object-based approach for urban land cover classification is presented in [19].

The approach presented in this paper utilizes both a pixel-based and object-based approach. Individual image pixels are first classified using a fuzzy classifier that makes use of both spectral and spatial information. The imagery is then segmented and features are derived from the segmentation image. The pixel classification is then used with additional object features to classify the image objects. By using an object-based fuzzy logic approach in addition to the per-pixel fuzzy classification, additional information that was not available in the pixel-based classification can be identified and used to improve the overall urban land cover classification result.

The remainder of this paper is organized as follows. A pixel-based hierarchical fuzzy classification technique that utilizes both spectral and spatial information to produce urban land cover maps is summarized in Section II and compared to the standard maximum-likelihood classification approach. The image segmentation method used in this study is presented in Section III. The segmented image is then classified by incorporating the results of the fuzzy pixel-based classification, shape and neighborhood information from the segmented image, and the raw multispectral image data. This methodology and corresponding results are presented in Section IV. Finally, the conclusions are presented in Section V.

II. Hierarchical Pixel-Based Fuzzy Classification

Here we briefly summarize the hierarchical pixel-based fuzzy classification approach and results that are used as input to the object-based classifier described in subsequent sections. Additional details of the pixel-based fuzzy classification methodology and results can be found in [4] and [20]. The imagery used for this study is an IKONOS image dataset of Columbia, MO, acquired on April 30, 2000. IKONOS images contain four multispectral bands with 4-m resolution (red, green, blue, and near infrared) and a panchromatic band with 1-m resolution. In our study, we fused the panchromatic band with the multispectral bands using a color normalization method [21] to produce a four-band pan-sharpened multispectral (PS-MS) image with 1-m resolution.

The urban land cover classes used in the pixel-based classification were *Road*, *Building*, *Grass*, *Tree*, *Bare Soil*, *Water*, and *Shadow*. Several of the land-cover classes, such as the *Road*/*Building* and *Tree*/*Grass* classes, are spectrally similar and have a significant amount of spectral overlap. To combat this problem, the fuzzy pixel-based classifier makes use of spatial information in addition to spectral information to help discriminate between spectrally similar classes. The entropy texture feature, calculated using a 10×10 occurrence window [22], was found to greatly increase the discrimination between the *Grass* and *Tree* classes. To discriminate between the *Road* and *Building* classes, a contextual feature measuring the spatial dimensions of spectrally similar groups of connected pixels was used. A simple algorithm was used to extract the length and width of spectrally similar connected groups of pixels from the PS-MS imagery, resulting in a two-band length-width feature image. These two features were found to reduce the number of misclassifications between the *Road* and *Building* classes.

The hierarchical pixel-based fuzzy classifier allows individual pairs of classes to be classified using only the spatial features best suited for those classes. The fuzzy classifier makes use of a maximum-likelihood classification to partition the PS-MS data into four sets: *Grass-Tree*, *Road-Building*, *Water-Shadow*, and *Bare Soil*. A membership value for each class in each set is then calculated from membership functions generated from the PS-MS data plus the appropriate spatial measure, entropy for the *Grass-Tree* set and length-width for the *Road-Building* set. Gaussian-shaped membership functions are used to represent both the PS-MS and entropy data, while the membership functions for the length-width contextual features are learned using a multilayer perceptron neural network trained using the standard back-propagation algorithm. After the calculation of membership in each of the classes, the *max* operator is used for defuzzification to generate a crisp classification.

Both maximum-likelihood classification and the fuzzy hierarchical classifier were applied to the IKONOS dataset. An accuracy assessment of the resulting classification was performed making use of reference pixels that were independent of the pixels used to train the classifier. The class accuracies for the hierarchical fuzzy and maximum-likelihood classifications are shown in Table I. There is an increase of at least 10%, and up to 25%, in class accuracy for all classes except *Bare Soil*, which remained at 96%. An urban image subset is shown in Fig. 1 and the corresponding maximum-likelihood and hierarchical fuzzy classifications are shown in Figs. 2 and 3, respectively.

III. Image Segmentation

The fuzzy pixel-based classification approach produces a classification map that is more accurate than the maximum-likelihood classifier by allowing different sets of classes to be classified using different spatial features in a hierarchical format. However, there are still significant classification errors in dense urban areas (Fig. 3). In the present urban land cover map, all man-made structures are classified as either *Road* or *Building*. In suburban areas, this scheme is appropriate as

TABLE I
COMPARISON OF URBAN LAND COVER CLASS ACCURACIES FOR MAXIMUM-LIKELIHOOD CLASSIFIER AND HIERARCHICAL PIXEL-BASED FUZZY CLASSIFIER

Class	Maximum Likelihood Classifier (%)	Hierarchical Fuzzy Classifier (%)
Road	70.6	88.3
Building	72.8	83.9
Grass	84.2	95.0
Tree	89.1	99.5
Bare Soil	96.0	96.0
Water	69.2	94.8

Fig. 1. One-meter resolution panchromatic IKONOS image subset of dense urban area.

Fig. 2. Maximum-likelihood classification of dense urban image shown in Fig. 1.

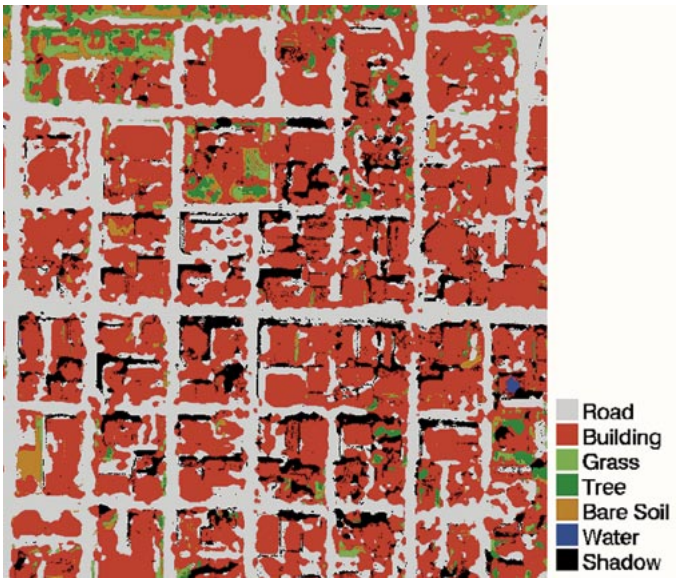

Fig. 3. Crisp output of fuzzy classifier for dense urban image shown in Fig. 1.

residential homes and streets dominate the landscape. However, in more dense urban areas, there are significant amounts of nonroad impervious surface land cover, such as parking lots and large sidewalks, and it is very desirable to differentiate between these surfaces and buildings. The fuzzy classifier is unable to correctly identify these areas because they are so spectrally similar to both the *Road* and *Building* classes. Here we adopt a segmentation and object-based classification approach to further refine the fuzzy pixel-based urban classification by adding an *Impervious Surface* class to identify nonroad, nonbuilding impervious surface. Because this land cover class is not found to a large extent in residential areas, and the fuzzy classifier performs well in those areas, the rest of this paper will focus on the classification of dense urban areas only.

The image segmentation algorithm used in this study follows the approach given in [13] where the segmentation is accomplished by region merging. The segmentation is initialized with each pixel in the image as a separate segment, and as the procedure progresses segments are merged together. The decision to merge two segments together is based on the increase in heterogeneity of the new segment, h_{diff}, when compared to its constituent segments. In order to allow a merge, the increase in heterogeneity must be less than a user set value, h_s, called the scale parameter. As h_s is increased, the size of segments found in an image will increase. The procedure stops when there are no possible merges with a value of h_{diff} less than h_s. The method used for finding two potential segments for a merge is local mutual best fitting. For a segment A, a neighboring segment B is found that has the smallest value of h_{diff} with A. For segment B, the neighboring segment C is found that has the smallest value of h_{diff} with B. If segment C and segment A are the same segment then segment B is the local mutual best fit for A. If not, then segment B replaces segment A and segment C replaces segment B and the procedure is repeated until the two local mutual best fitting segments are found.

Different measures of heterogeneity can be used that take into account both spectral and shape heterogeneity. Here, the spectral variance of each multispectral channel in the segment is

used to measure spectral heterogeneity, and the ratio of the segment's perimeter length to the perimeter length of a square containing the same number of pixels is used to measure shape heterogeneity. These heterogeneity measures favor segments with minimal spectral variance and compact shape. The increase in heterogeneity when two segments are merged is calculated as

$$h_{\text{diff}} = \sum_{q=1}^{m+1} w_q \left(n_1 \left(h_{\text{mq}} - h_{1q} \right) + n_2 \left(h_{\text{mq}} - h_{2q} \right) \right) \quad (1)$$

where h_{mq} is the resultant heterogeneity of the merged segment for heterogeneity measure q; h_{1q} and h_{2q} are the heterogeneities for the two segments being merged for measure q; n_1 and n_2 are the number of pixels in each of the two segments being merged; and w_q is the weight for each heterogeneity measure. The weight determines the influence of each heterogeneity measure to the total increase in heterogeneity h_{diff}. For the specific case of IKONOS image data with four spectral channels $m = 4$ for the heterogeneity measures described above. The parameters h_{mq}, h_{1q}, h_{2q}, and w_q for $q = 1 - 4$ are the spectral heterogeneity measures and weights, and h_{m5}, h_{15}, h_{25}, and w_5 are the spatial heterogeneity measures and their weight.

The region-growing segmentation algorithm was applied to the IKONOS image and a subset of this showing the segmentation of a dense urban area (Fig. 1) is shown in Fig. 4. These results were obtained using a scale parameter $h_s = 700\,000$ and weights $w_q = 1$ for $q = 1 - 4$ and $w_5 = 400$. Although the weight for the shape heterogeneity measure is much larger than the weights for the spectral heterogeneity measures, shape heterogeneity has less of an impact on h_{diff} than spectral heterogeneity because the increase in spectral heterogeneity when two segments are merged is much larger than the increase in shape heterogeneity. IKONOS imagery has very low contrast, and it was found that if the image is histogram equalized before segmentation, the segmentation results were greatly improved. While many of the road and impervious surface regions in the image are broken into multiple segments, the segmentation successfully segments most of the buildings in the image as single segments. From this segmentation image it is then possible to use an object-based classification approach to differentiate between the *Building* and *Impervious Surface* classes.

IV. Object-Based Fuzzy Classification of the Segmented Image

Once a successfully segmented image is obtained, it is possible to apply an object-based fuzzy logic classification to the segmentation image to assign a class label to each of the segments. Because we are dealing with image segments instead of pixels, object features such as shape and neighborhood information are available for use in the classification that were not available in the pixel-based fuzzy classifier. In addition, spectral statistics such as the mean and variance of the pixels in each segment can be calculated. Because the image has already been classified on a per-pixel basis, an initial fuzzy classification of the image segments can be performed by analyzing the classes of the constituent pixels in each segment.

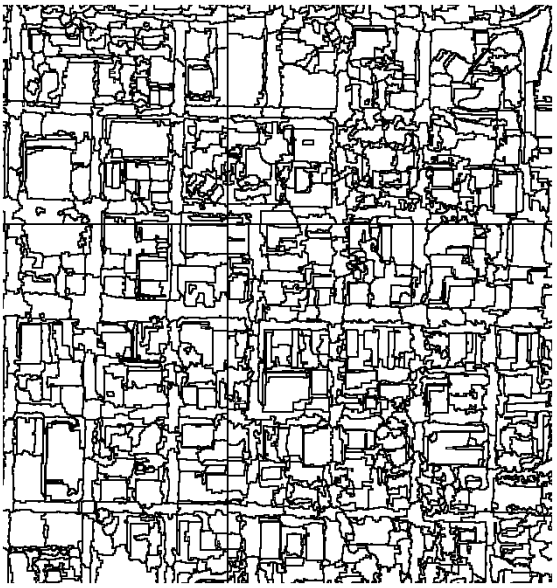

Fig. 4. Segmentation of dense urban image shown in Fig. 1.

The goal of using an object-based approach at this stage in the processing is to improve the urban land cover classification in dense urban areas by discriminating between buildings and nonroad impervious surface. This was not possible with the maximum-likelihood or the fuzzy pixel-based approaches. The strategy employed for the discrimination between the *Building* and *Impervious Surface* classes is to label all pixels classified as *Building* from the fuzzy pixel-based classification as *Impervious Surface* and use subsequent object-based classification techniques to identify *Building* segments from within the *Impervious Surface* class. The object features used to identify *Building* segments are the classes of the constituent pixels that make up the segment, morphological shape information, location of potential *Building* segments with respect to *Shadow* segments, mean panchromatic brightness values of the segment, and multispectral mean and variance values from the PS-MS data in each segment. Based on these object features, a fuzzy logic rule base is used to discriminate between *Building* and *Impervious Surface* segments.

A. Fuzzy Membership of Image Objects From Pixel Class

Initially, fuzzy membership values in each class are calculated for the segments based on the proportion of each class present in the segments from the per-pixel image classification. All pixels classified as *Building* from the fuzzy pixel classification are changed to *Impervious Surface* so the segments initially have no membership in the *Building* class. Subsequent object-based processing is utilized to identify *Building* segments from segments with a high membership value in the *Impervious Surface* class. An S-function is used to calculate the membership values of a segment in each of the classes. First, the percentage, p_i, of each class present in the segment is calculated from the classification image, where $i = 1, \ldots, n_c$, and n_c is the number of classes. The membership value in each class $\mu_{c,i}(p_i)$ is calculated from the S-function as

$$\mu_{c,i}\left(p_i\right) = S\left(p_i; 0.0, 0.5, 1.0\right) \quad (2)$$

where

$$S(x;a,b,c)=\begin{cases}0, & \text{for } x\le a\\ \frac{1}{2}\left(\frac{x-a}{b-a}\right)^2, & \text{for } a<x\le b\\ 1-\frac{1}{2}\left(\frac{x-c}{c-b}\right)^2, & \text{for } b<x\le c\\ 1, & \text{for } x>c.\end{cases} \tag{3}$$

Segments consisting of pixels primarily from one class have membership values close to one in that class and membership values close to zero in the other classes. Segments containing proportionately large numbers of pixels in several classes have no membership values close to one in any of the classes, reflecting the ambiguity of the information extracted from the pixel classifications in the segment. The subscript c in $\mu_{c,i}(p_i)$ indicates that these membership values were calculated from the per-pixel classification of the image segments.

B. Morphological Shape Processing

Shape information for each segment is measured using the morphological skeleton of the segment. Morphological skeletonization is a process for reducing a binary shape, in this case a single segment, to a graph that largely preserves the extent and connectivity of the segment while discarding the foreground pixels in the segment. While a wide variety of skeletonizing algorithms exist, all do not, however, guarantee the production of a connected skeleton [22]. The skeletonizing algorithm used here is based on a morphological thinning procedure and is guaranteed to produce a connected and one-pixel-thick skeleton [23]. The skeleton is found by cyclically applying morphological thinning operations to the segment until no further thinning is possible. The segment is iteratively thinned with eight structuring elements during each thinning cycle. The structuring elements used for the thinning are

0	0	0
	1	
1	1	1

	0	0
1	1	0
	1	

and their 90° rotations. The ones are the foreground, and the zeros are the background elements of the structuring elements. During each thinning iteration, all eight structuring elements are individually passed over the segment as a convolutional mask, thereby removing the pixel at the center of the structuring element if the pixels of the segment exactly match the background and foreground elements of the structuring element. This skeleton is very sensitive to small variations in the boundary of the original segment. In order to minimize the sensitivity to boundary variations, the original segments are initially smoothed by performing a morphological closing operation using a five-pixel diameter disk-structuring element.

After the skeleton has been extracted from the segment, the endpoints of the skeleton are identified. Line segments are then found to connect the skeleton endpoints, and the angle between the two line segments connected to each endpoint is calculated. This process is illustrated in Fig. 5. The angles and line segment lengths are used as shape information to help classify the segment. Buildings are modeled as segments that are approximately rectangular in shape and have a large membership value in the *Impervious Surface* class. An "approximately rectangular" segment is modeled as a segment with the following attributes: about four endpoints with angles close to 90° and large separation, about two or less endpoints with angles much larger than 90°, and about two or less endpoints with angle much smaller than 90°. Because the attributes of an "approximately rectangular" segment are imprecise and the shapes of buildings vary, fuzzy membership functions are used to measure how closely the endpoint angles and the line segment lengths between the endpoints match the different criteria.

First, three fuzzy membership values are calculated for each skeleton endpoint angle θ_i: about 90°, $\mu_{\sim 90}(\theta_i)$, larger than 90°, $\mu_{>90}(\theta_i)$, and smaller than 90°, $\mu_{<90}(\theta_i)$, where $i=1,\ldots,n_e$, and n_e is the number of endpoints in the segment skeleton. First, $\mu_{\sim 90}(\theta_i)$ is calculated using a π-function as

$$\mu_{\sim 90}(\theta_i)=\pi(\theta_i;70,80,85,95,100,110) \tag{4}$$

where

$$\pi(x;a,b,c,d,e,f)=\begin{cases}0, & \text{for } x\le a \text{ or } x\ge f\\ S(x;a,b,c), & \text{for } a<x<c\\ 1, & \text{for } c\le x\le d\\ 1-S(x;d,e,f), & \text{for } d<x<f.\end{cases} \tag{5}$$

Both $\mu_{>90}(\theta_i)$ and $\mu_{<90}(\theta_i)$ are calculated using S-functions as

$$\mu_{>90}(\theta_i)=S(\theta_i;95,100,110) \tag{6}$$

$$\mu_{<90}(\theta_i)=1-S(\theta_i;70,80,85). \tag{7}$$

The angle values controlling the shape of the membership functions in (4), (6), and (7) where chosen so that angles matching the description of the membership functions would have membership close to one, while angles deviating from the descriptions would have membership values approaching zero.

A membership value to quantify "large separation" between the skeleton endpoints, $\mu_{\rm LS}(e_i)$, $i=1,\ldots,n_e$, is calculated for each line segment connecting the segment skeleton endpoints as

$$\mu_{\rm LS}(e_i)=S(\min[d_i,d_{i+1}];3,5,7) \tag{8}$$

where e_i is the ith endpoint, and d_i is the distance between endpoints e_{i-1} and e_i. "Large separation" is defined in this case as being significantly larger than 5 m. To identify endpoints that have both angles near 90° and large separation, the fuzzy intersection of $\mu_{\sim 90}(\theta_i)$ and $\mu_{\rm LS}(e_i)$ is calculated using the $\min$ operator

$$\mu_{\sim 90,LS}(e_i)=\min[\mu_{\sim 90}(\theta_i),\mu_{\rm LS}(e_i)]. \tag{9}$$

Fuzzy quantifiers [24] are used to calculate membership values for fuzzy sets describing "about four" or "about two or less." The membership value for a segment having about four endpoints with angles close to 90° and large separation μ_4 is calculated as

$$\mu_4=\pi\left(\sum_{i=1}^{n_e}\mu_{\sim 90,LS}(e_i);1.0,1.5,2.5,5.5,6.5,7.0\right). \tag{10}$$

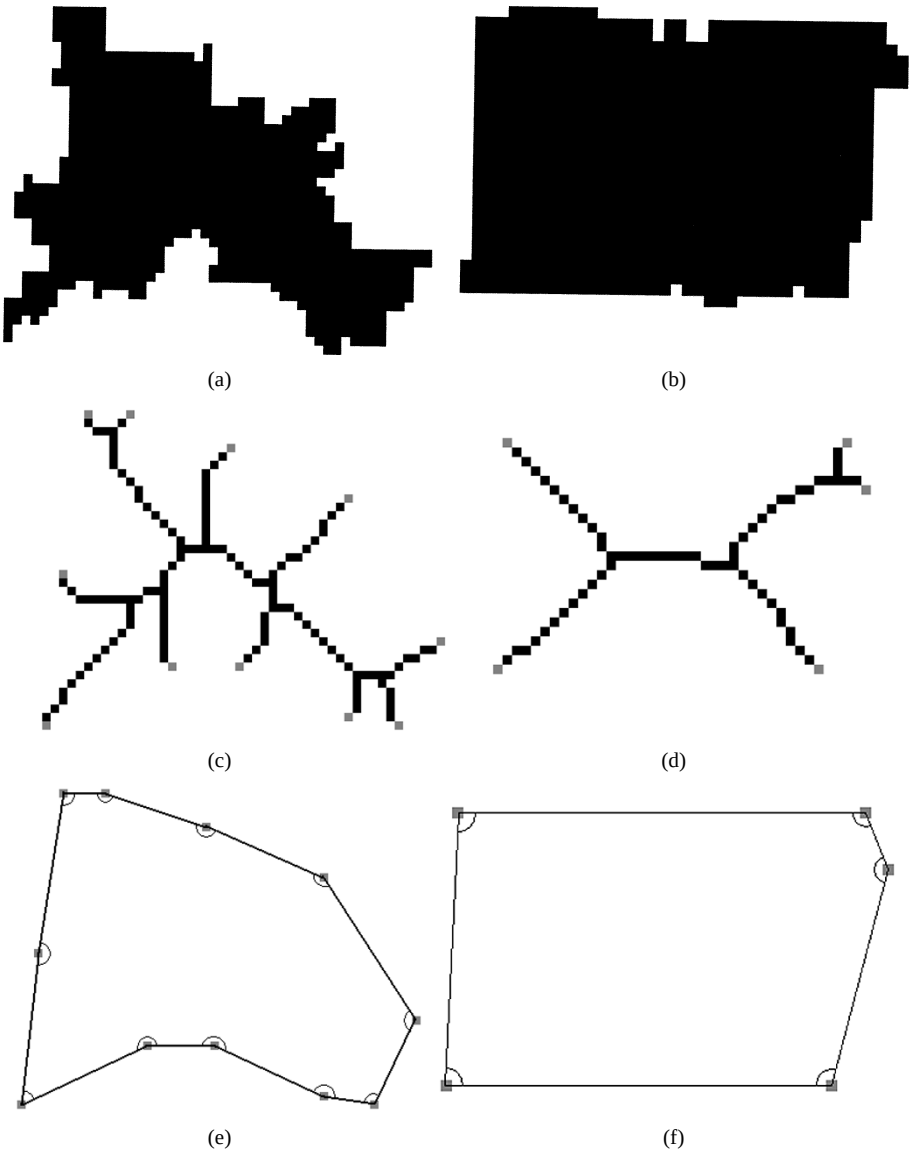

Fig. 5. Morphological skeleton processing for image segments shown in (a) and (b). Result of skeletonizing algorithm shown in (c) and (d) for image segments (a) and (b), respectively. The endpoints of the skeletons have been highlighted in gray. In (e) and (f), the skeleton endpoints have been connected by line segments and the endpoint angles identified.

The membership values for a segment having about two or less angles much larger than 90°, $\mu_{2>}$, and having about two or less angles much smaller than 90°, $\mu_{2<}$, are calculated as

$$\mu_{2>} = 1 - S\left(\sum_{i=1}^{n_e} \mu_{>90}(\theta_i); 2.0, 3.0, 4.5\right) \tag{11}$$

$$\mu_{2<} = 1 - S\left(\sum_{i=1}^{n_e} \mu_{<90}(\theta_i); 2.0, 3.0, 4.5\right). \tag{12}$$

Finally, the membership value for a segment being "approximately rectangular" μ_R is calculated using the fuzzy intersection of μ_4, $\mu_{2>}$, and $\mu_{2<}$ with the $\min$ operator,

$$\mu_R = \min\left[\mu_4, \mu_{2>}, \mu_{2<}\right]. \tag{13}$$

C. Segment Neighborhood Analysis

A common feature that buildings possess is that they cast shadows on the ground. The amount of shadows present in a high-resolution image will vary depending on the sun azimuth and elevation angles and the satellite sensor acquisition azimuth angle. As the sun elevation angle decreases from 90°, the length of the shadow buildings cast along the ground grows, and as the sun and sensor azimuth angles get further apart, the amount of shadows visible to the sensor will increase. If shadows are present in the image, they can be used to help identify *Building* segments. For the IKONOS image in this study the sun elevation angle was 61°, the sun azimuth angle was 139°, and the sensor azimuth angle was 352°. As a result, building shadows are prominent as seen in the image subset shown in Fig. 1. Also note that the shadows are for the most part well segmented (Fig. 4), thereby allowing successful neighborhood analysis.

The process for identifying segments as *Building* using neighborhood analysis of *Shadow* segments is as follows. First, segments with membership value of at least 0.5 in the *Shadow* class are identified. Then the segments bordering the potential *Shadow* segments in the direction of the sun azimuth angle are

extracted. Segments with high membership in the *Impervious Surface* class that share a border with these potential *Shadow* segment are likely *Building* segments. The search direction for segments neighboring potential *Shadow* segments must be quantized into one of eight directions because we are working on a digital image grid. Because of this, segments that are as much as 45° off the direction of the sun azimuth angle will be identified as potential *Building* segments. To avoid misclassifications, segments sharing a larger border along the direction of the sun azimuth angle with the potential *Shadow* segment are given higher membership values. The length of the border of each segment neighboring the *Shadow* segment in the direction of the sun azimuth angle is calculated and normalized by the largest border length. The membership value of the ith segment s_i bordering a *Shadow* segment is calculated as

$$\mu_S(s_i) = S\left(\frac{l_i}{l_{\max}}; 0.4, 0.6, 0.8\right) \tag{14}$$

where l_i is the length of the border shared with the *Shadow* segment, and $l_{\max}$ is the length of the largest border shared with the *Shadow* segment. The μ_S membership value is calculated for all segments bordering a segment in the direction of the sun azimuth angle with membership in the *Shadow* class of at least 0.5.

D. Spectral Object Features

While many buildings are spectrally similar to various impervious surface ground covers, some do have unique spectral signatures and can be identified from spectral features calculated from the constituent pixels within a segment. The spectral features calculated for the ith band of the pixels in the segment are the mean m_i and the variance σ_i^2. A number of the buildings in the image have very bright spectral responses, and a fuzzy membership function quantifying the brightness in the panchromatic band $\mu_{\mathrm{PAN}}(m_p)$ can be used to identify buildings of this type. Here m_p is the mean value of the panchromatic band of the pixels in the segment

$$\mu_{\mathrm{PAN}}(m_p) = S(m_p; 400, 550, 700). \tag{15}$$

Image segments with a large mean value in the panchromatic band will have membership close to one in μ_{PAN}. The values governing the fuzzy membership function to identify a bright response in the panchromatic band were chosen by examining the spectral response of typical buildings that could be identified in this manner. Although these values were set manually, they could easily be calculated from training data.

Some buildings in the imagery, while they do not have a bright response in the panchromatic band, do have a unique spectral response in the multispectral bands, allowing for discrimination between the *Building* and *Impervious Surface* classes for these segments. Fuzzy membership functions for each multispectral band are defined using the mean $m_{t,i}$ and variance, $\sigma_{t,i}^2$, calculated from *Building* training data, where $i = 1, \ldots, m$, and m is the number of multispectral bands. The membership value $\mu_{\mathrm{MS},i}$ for the segment in each band is calculated using

$$\mu_{\mathrm{MS},i}(m_i) = \pi(m_i; a, b, c, d, e, f) \tag{16}$$

where $a = m_{t,i} - 0.8\sigma_{t,i}$, $b = m_{t,i} - 0.5\sigma_{t,i}$, $c = m_{t,i} - 0.3\sigma_{t,i}$, $d = m_{t,i} + 0.3\sigma_{t,i}$, $e = m_{t,i} + 0.5\sigma_{t,i}$, and $f = m_{t,i} + 0.8\sigma_{t,i}$.

The parameters controlling the shape of the membership function were chosen such that segments with a mean value within one-half of a standard deviation of the training data mean will have membership greater than 0.5. The membership values $\mu_{\mathrm{MS},i}$ indicate the degree of similarity between a segment and the *Building* training data for each multispectral band. These values are combined to form a single fuzzy membership for the segment μ_{MS} by calculating the fuzzy intersection of the m membership values for the individual bands

$$\mu_{\mathrm{MS}} = \min[\mu_{\mathrm{MS},1}, \ldots, \mu_{\mathrm{MS},m}]. \tag{17}$$

Both μ_{PAN} and μ_{MS} are calculated for each image segment, indicating the degree of membership in the *Building* class in terms of the panchromatic and multispectral data, respectively.

E. Fuzzy Logic Classification of Object Features

The object membership values for the different *Building* attributes, μ_R, μ_S, μ_{PAN}, μ_{MS}, and $\mu_{c,i}$, $i = 1, \ldots, m$, are calculated for each segment in the image. Segments that do not border a potential *Shadow* segment have μ_S set to zero. The identification of *Building* segments is accomplished with the use of a fuzzy logic rule base. The rule base used to calculate the membership value in the *Building* and *Impervious Surface* classes for the ith segment in the image, s_i, is defined as follows.

- R1: If s_i *Impervious Surface* membership is high AND s_i is approximately rectangular, then s_i membership in *Potential Building* is high.
- R2: If s_i *Impervious Surface* membership is high AND s_i borders *Shadow* AND *Shadow* membership of bordering segment is high, then s_i membership in *Potential Building* is high.
- R3: If s_i *Impervious Surface* membership is high AND s_i has bright panchromatic response, then s_i membership in class *Potential Building* is high.
- R4: If s_i *Impervious Surface* membership is high AND s_i has *Building* multispectral response, then s_i membership in class *Potential Building* is high.
- R5: If **R1** OR **R2** OR **R3** OR **R4** is high, then s_i membership in class *Building* is high.
- R6: If s_i *Impervious Surface* membership is high AND s_i *Building* membership is NOT high, then s_i membership in *Impervious Surface* is high.

There are a variety of operators in fuzzy systems that can be used to implement the fuzzy "AND," "OR," and "NOT." The $\min$ and $\max$ operators are used for "AND" and "OR," respectively, and the standard fuzzy compliment [25] is used for "NOT." The fuzzy rule base is implemented as

$$\mu_{R,B}(s_i) = \min[\mu_{c,I.S.}(s_i), \mu_R(s_i)] \tag{18}$$

$$\mu_{S,B}(s_i) = \min[\mu_{c,I.S.}(s_i), \mu_S(s_i), \mu_{c,S}(s_{\mathrm{sdw}})] \tag{19}$$

$$\mu_{\mathrm{PAN},B}(s_i) = \min[\mu_{c,I.S.}(s_i), \mu_{\mathrm{PAN}}(s_i)] \tag{20}$$

$$\mu_{\mathrm{MS},B}(s_i) = \min[\mu_{c,I.S.}(s_i), \mu_{\mathrm{MS}}(s_i)] \tag{21}$$

TABLE II
CLASSIFICATION ACCURACIES FOR DIFFERENT COMBINATIONS OF OBJECT-BASED FEATURES

Feature Combination	*Building* Accuracy (%)	*Impervious Surface* Accuracy (%)	Average Accuracy of *Building* and *Imp. Surf.* (%)
Shape	24.9	87.4	56.2
Shadow	30.2	91.4	60.8
Pan	10.8	92.0	51.4
MS	32.0	84.4	58.2
MS + Pan	38.9	84.4	61.7
Shape + MS + Pan	54.9	81.0	68.0
Shadow + MS + Pan	64.5	83.8	74.2
Shape + Shadow + MS + Pan	76.1	81.0	78.6

$$\mu_{c,\text{Building}}(s_i) = \max[\mu_{R,B}(s_i), \mu_{S,B}(s_i), \mu_{\text{PAN},B}(s_i), \mu_{\text{MS},B}(s_i)] \quad (22)$$

$$\mu_{c,\text{Impervious Surface}}(s_i) = \min[\mu_{c,I.S.}(s_i), 1 - \mu_{c,\text{Building}}(s_i)] \quad (23)$$

where $\mu_{c,S}(s_{\text{sdw}})$ is the membership in the *Shadow* class of the segment bordering the segment being examined in the direction of the sun azimuth angle. The result of this processing is a fuzzy classification of the image segments, with each segment having membership values $\mu_{c,j}$ in each of the eight classes: *Road*, *Building*, *Impervious Surface*, *Grass*, *Tree*, *Bare Soil*, *Water*, and *Shadow*. Since a crisp classification is desired, the fuzzy classification must be defuzzified to produce a single class label for each image segment. Defuzzification is performed using the max operator such that segment s_i is classified as the class c with the highest membership value

$$\text{Class}(s_i) = \arg\max_{j=1}^{8}\{\mu_{c,1}(s_i), \ldots, \mu_{c,8}(s_i)\}. \quad (24)$$

F. Object-Based Fuzzy Classification Results

The object-based fuzzy classification scheme was applied to the IKONOS image from Columbia, Missouri. The inputs to the classifier were the pixel-based fuzzy classification, and the panchromatic and PS-MS images. The prototype vectors used for training the *Building* multispectral fuzzy sets were the same used in training the pixel-based classifier. After the image was segmented, the object-based classification proceeded as described above. An accuracy assessment of the resulting classification was performed making use of reference pixels that were independent of the pixels used for training. The reference pixel datasets were generated via photo interpretation of the PS-MS IKONOS imagery. Approximately 130 randomly distributed test site polygons were manually digitized in the imagery. The dataset had 1291 training pixels and 51 368 reference pixels. Because this classification scheme was designed for the analysis of urban areas, the reference sites used for the accuracy assessment were all drawn from dense urban areas in the imagery. These areas had very few *Bare Soil* and *Water* pixels, so no reference pixels were identified for those classes.

When each of the four object features was used separately to identify *Building* segments, only a fraction of the buildings were correctly identified. However, when all four were used in conjunction, 76% of the *Building* reference pixels were properly identified, while still correctly identifying 81% of the *Impervious Surface* reference pixels. Table II summarizes the effect of using different combinations of the object features on the accuracy of the *Building* and *Impervious Surface* classification. The single most effective object feature for discrimination between the *Building* and *Impervious Surface* classes is multispectral information, which correctly classifies 32% of the *Building* reference pixels. The *Building* class accuracy does not rise above 50% until at least three of the information sources are used. The results in Table II show that all four object-based features contribute to the identification of *Building* segments and each provide complimentary information. As the number of features is increased, the accuracy of the *Impervious Surface* class decreases. This occurs because the number of *Impervious Surface* pixels that are misclassified as *Building* increases as the number of correctly identified *Building* reference pixels increases. However, the average accuracy of the *Building* and *Impervious Surface* classes increases with the number of features, increasing the overall accuracy of the classification.

The confusion matrix for the object-based classification of the dense urban image utilizing all four features is given in Table III. The *Road* class is very accurate with 99% of *Road* reference pixels correctly classified as *Road*. The *Road* class accuracy is increased by almost 11% when using the object-based classifier as compared to the pixel-based classifier (see Table I). Because the membership values of a segment calculated from the pixel-based classification are based on the proportional numbers of pixels of each class present in a segment, the segmentation operates as a majority filter [25] if the segment is dominated by a single class. Misclassifications between the *Building* and *Impervious Surface* classes are the largest source of error with 19% of *Building* reference pixels misclassified as *Impervious Surface*, and 11% of *Impervious Surface* reference pixels misclassified as *Building*. Comparing this to the pixel-based fuzzy classifier accuracies reported in Table I, the *Building* class accuracy appears to have decreased, dropping from 84% to 76%. It should be noted, however, that for dense urban areas, like the one shown in Fig. 1, the *Building* class accuracy reported for the pixel-based fuzzy classifier is an overestimate as there is no *Impervious Surface* class included in that classification

TABLE III
CONFUSION MATRIX FOR OBJECT-BASED CLASSIFICATION OF DENSE URBAN AREA

	Road Ref.	*Building* Ref.	*Imp. Surf.* Ref	*Grass* Ref.	*Tree* Ref.	Total	%
Road	10164	499	826	0	0	11489	88.5
Building	0	7845	1137	0	0	8982	87.3
Imp. Surf.	86	1959	8343	0	13	10401	80.2
Grass	0	0	0	9330	0	9330	100.0
Tree	0	0	0	887	10279	11166	92.6
Total	10250	10303	10306	10217	10292	51368	
%	99.2	76.1	81.0	91.3	99.9		86.4

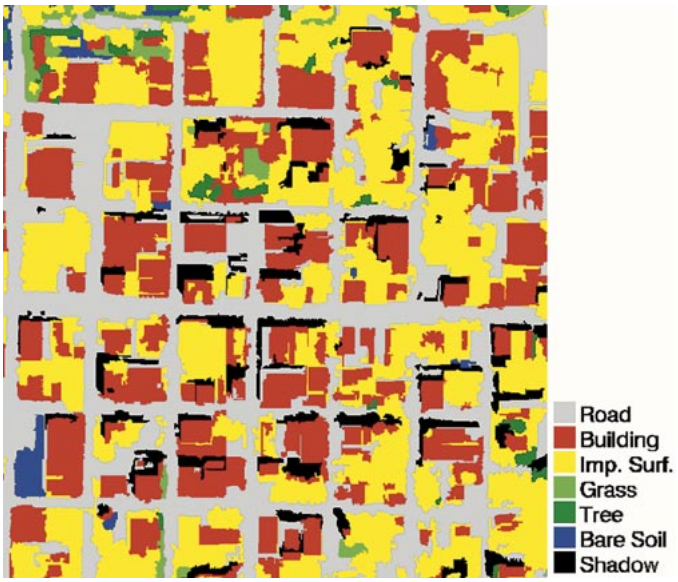

Fig. 6. Object-based classification of dense urban area shown in Fig. 1 using segmentation image shown in Fig. 4 and fuzzy-logic pixel-based classification shown in Fig. 3.

scheme and nonroad, nonbuilding impervious surface makes up a significant portion of the landscape in dense urban areas. The object-based fuzzy classifier produces a more detailed urban land-cover classification by including both a *Building* class and an *Impervious Surface* class. The classification image generated using this technique is shown in Fig. 6. Note the significant improvement in both the *Road* and *Building* classes relative to the maximum-likelihood and pixel-based fuzzy classifier results shown in Figs. 2 and 3, respectively, for the same dense urban area.

V. CONCLUSION

In this paper we presented a combined fuzzy pixel-based and object-based approach for classification of urban land cover from high-resolution multispectral image data. First a pixel-based hierarchical fuzzy classifier was described that utilizes both spectral and spatial information to classify individual image pixels. The fuzzy classifier improved the classification accuracies over the maximum-likelihood classification by 10% to 25%. Next, a multiresolution segmentation technique that utilized both spectral and spatial heterogeneity was used to segment the image to facilitate further object-based classification. Using an object-based fuzzy logic classification approach, we produced a more detailed classification map by differentiating between the *Building* and nonroad *Impervious Surface* classes in a dense urban environment that was not possible using pixel-based classifiers. Several information sources were used by the object-based classifier that were not available in the pixel-based approach. They were shape information from the segments, segment neighborhood analysis, and spectral statistics of the object. Using these techniques, the object-based fuzzy logic classifier was able to identify *Buildings* with a 76% accuracy and *Impervious Surface* with an 81% accuracy. The fuzzy logic approach presented here is flexible in that more object features can be easily added to the rule base. Further work is needed on the decision rules for the identification of the *Building* segments to include features and rules to discriminate between different types of buildings, such as residential, commercial, and industrial.

REFERENCES

[1] USGS, "The National Map," United States Geological Survey, USGS Fact Sheet 101–01, 2001.
[2] J. R. Jenson, *Introductory Digital Image Processing: A Remote Sensing Perspective*, 2nd ed. Upper Saddle River, NJ: Prentice-Hall, 1996.
[3] C. H. Davis and X. Wang, "Urban land cover classification from high resolution multi-spectral IKONOS imagery," in *Proc. IGARSS*, vol. 2, Toronto, ON, Canada, June 24–28, 2002, pp. 1204–1206.
[4] A. K. Shackelford and C. H. Davis, "A fuzzy classification approach for high-resolution multispectral data over urban areas," in *Proc. IGARSS*, vol. 3, Toronto, ON, Canada, June 24–28, 2002, pp. 1621–1623.
[5] A. Bardossy and L. Samaniego, "Fuzzy rule-based classification of remotely sensed imagery," *IEEE Trans. Geosci. Remote Sensing*, vol. 40, pp. 362–374, Feb. 2002.
[6] F. Melgani, B. A. R. AL Hashemy, and S. M. R. Taha, "An explicit fuzzy supervised classification method for multispectral remote sensing images," *IEEE Trans. Geosci. Remote Sensing*, vol. 38, pp. 287–295, Jan. 2000.
[7] A. J. Tatem, H. G. Lewis, P. M. Atkinson, and M. S. Nixon, "Super-resolution mapping of urban scenes from IKONOS imagery using a Hopfield neural network," in *Proc. IGARSS*, vol. 7, 2001, pp. 3203–3205.
[8] F. Dell'Acqua and P. Gamba, "Detection of urban structures in SAR images by robust fuzzy clustering algorithms: The example of street tracking," *IEEE Trans. Geosci. Remote Sensing*, vol. 39, pp. 2287–2297, Oct. 2001.
[9] I. Couloigner and T. Ranchin, "Mapping of urban areas: A multiresolution modeling approach for semi-automatic extraction of streets," *Photogramm. Eng. Remote Sens.*, vol. 66, no. 7, pp. 867–874, July 2000.
[10] C. Steger, "An unbiased detector of curvilinear structures," *IEEE Trans. Pattern Anal. Machine Intell.*, vol. 20, pp. 113–125, Feb. 1998.
[11] M. Pesaresi, "Textural classification of very high-resolution satellite imagery: Empirical estimation of the interaction between window size and detection accuracy in urban environment," in *Proc. ICIP*, vol. 1, 1999, pp. 114–118.
[12] C. Evans, R. Jones, I. Svalbe, and M. Berman, "Segmenting multispectral Landsat TM images into field units," *IEEE Trans.Geosci. Remote Sensing*, vol. 40, pp. 1054–1064, May 2002.

[13] M. Baatz and A. Schape, "Multiresolution segmentation: An optimization approach for high quality multi-scale image segmentation," in *Angewandte Geographische Informationsverabeitung. XII. Beitrage zum AGIT-Symp. Salzburg 2000*, T. Strobl, T. Blaschke, and G. Griesebner, Eds., Karlsruhe, 2000, pp. 12–23.

[14] J. C. Tilton, "Image segmentation by region growing and spectral clustering with a natural convergence criterion," in *Proc. IGARSS*, vol. 4, Seattle, WA, July 6–10, 1998, pp. 1766–1768.

[15] C. Mott, T. Anderson, S. Zimmermann, T. Schneider, and U. Ammer, "Selective region growing—An approach based on object-oriented classification routines," in *Proc. IGARSS*, vol. 3, Toronto, ON, Canada, June 24–28, 2002, pp. 1612–1614.

[16] A. Sarkar, M. K. Biswas, B. Kartikeyan, V. Kumar, K. L. Majumder, and D. K. Pal, "An MRF model-based segmentation approach to classification for multispectral imagery," *IEEE Trans. Geosci. Remote Sensing*, vol. 40, pp. 1102–1113, May 2002.

[17] M. Pesaresi and J. A. Benediktsson, "A new approach for the morphological segmentation of high-resolution satellite imagery," *IEEE Trans. Geosci. Remote Sensing*, vol. 39, pp. 309–320, Feb. 2001.

[18] J. A. Benediktsson, K. Arnason, and M. Persaresi, "The use of morphological profiles in classification of data from urban areas," in *Proc. IEEE/ISPRS Joint Workshop of Remote Sensing and Data Fusion over Urban Areas*, Nov. 2002, pp. 30–34.

[19] R. P. Kressler, T. B. Bauer, and K. T. Steinnocher, "Object-oriented per-parcel land use classification of very high resolution images," in *Proc. IEEE/ISPRS Joint Workshop on Remote Sensing and Data Fusion over Urban Areas*, Nov. 2002, pp. 164–167.

[20] A. K. Shackelford and C. H. Davis, "A hierarchical fuzzy classification approach for high-resolution multispectral data over urban areas," *IEEE Trans. Geosci. Remote Sensing*, vol. 41, pp. 1920–1932, Sept. 2003.

[21] J. Vrabel, "Multispectral imagery advanced band sharpening study," *Photogramm. Eng. Remote Sens.*, vol. 66, no. 1, pp. 73–79, Jan. 2000.

[22] R. C. Gonzalez and R. E. Woods, *Digital Image Processing*, 2nd ed. Upper Saddle River, NJ: Prentice-Hall, 2002.

[23] B. K. Jang and R. T. Chin, "Analysis of thinning algorithms using mathematical morphology," *IEEE Trans. Pattern Anal. Machine Intell.*, vol. 12, pp. 541–551, June 1990.

[24] G. J. Klir and B. Yuan, *Fuzzy Sets and Fuzzy Logic: Theory and Applications*. Upper Saddle River, NJ: Prentice-Hall, 1995.

[25] P. Maragos and L. F. C. Pessoa, "Morphological filtering for image enhancement and detection," in *Handbook of Image and Video Processing*, A. Bovik, Ed. San Diego, CA: Academic, 2000, pp. 101–116.

Aaron K. Shackelford (S'97) was born in Kansas City, MO, on January 1, 1977. He received the B.S. and M.S. degrees in electrical engineering from the University of Missouri-Columbia, Columbia, in 1999 and 2001, respectively. He is currently pursuing the Ph.D. degree in electrical engineering from the University of Missouri-Columbia.

Since January of 2000, he has been a Research Assistant in the Department of Electrical Engineering, University of Missouri-Columbia. He was a Research Scholar in the Department of Electronic Engineering, City University of Hong Kong, Hong Kong, for three months in 2000. He is currently a Research Assistant in the Remote Sensing Laboratory, University of Missouri-Columbia. His research interests include application of pattern recognition approaches to remote sensing imagery and patch antenna design.

Mr. Shackelford is a member of Tau Beta Pi. He was awarded the NASA Graduate Student Researchers Program fellowship in 2001.

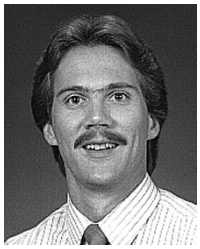

Curt H. Davis (S'90–M'92–SM'98) was born in Kansas City, MO, on October 16, 1964. He received the B.S. and Ph.D. degrees in electrical engineering from the University of Kansas, Lawrence, in 1988 and 1992, respectively.

He has been actively involved in experimental and theoretical aspects of microwave remote sensing of the ice sheets since 1987. He has participated in two field expeditions to the Antarctic continent and one to the Greenland ice sheet. From 1989 to 1992, he was a NASA Fellow at the Radar Systems and Remote Sensing Laboratory, University of Kansas where he conducted research on ice-sheet satellite altimetry. He is currently the Croft Distinguished Professor of Electrical and Computer Engineering at the University of Missouri-Columbia. His research interests are in the areas of mobile radio signal propagation, RF/microwave systems, satellite remote sensing, and remote sensing applications for urban environments.

Dr. Davis is a member of the Tau Beta Pi, Eta Kappa Nu, and URSI-Commission F. He is a former Chairman of the Instrumentation/Future Technologies committee of the IEEE Geoscience and Remote Sensing Society. In 1996, he was selected by the International Union of Radio Science for their Young Scientist Award. He was awarded the Antarctica Service Medal from the National Science Foundation.

Special Issue Communications

A Physics-Based Parametric Representation of the Wind Direction Signal in Sea Surface Microwave Brightness Temperatures

Eric Baum and Bruce Hauss

***Abstract*—Polarimetric passive measurements of sea surface brightness temperature have been proposed as a means of inferring wind speed and direction. A limited set of circle flight measurements of the wind direction dependence has demonstrated that there may be enough independent information in the polarimetric measurement to make this feasible. A predictive model by Yueh reproduces the observations closely enough that the dominant mechanisms are probably included. Optimizing the fit of this type of model with a growing dataset is made difficult by the close coupling of the Yueh approach with a particular wind–wave spectral model. This makes it unclear as to how to parameterize the model, a prerequisite of any systematic optimization technique. Here, we present an alternate formulation, using the Baum–Irisov model to isolate the particular properties of the wavy ocean surface that affect the radiance, in the form of six discrete parameters. Iterative local linearization techniques are used to optimize the values of these parameters with respect to any large dataset. The parameters are functions of only two variables (radiometer frequency and wind speed), while the effects of incidence angle, polarization, sea surface temperature, salinity, and wind direction are derived from the model. Since the data need only be binned by these two variables, a relatively small number of on-orbit/ground-truth datasets is required to evaluate the parameters.**

***Index Terms*— Microwave, ocean, radiometry, wind.**

I. Introduction

A conventional two-scale description of radar back-scatter from the ocean surface includes the Bragg-resonant contribution to diffractive scattering obtained from a small perturbation theory [3] along with a Gaussian slope probability density function (pdf) to describe the effect of the unresolved tilting of the surface by waves which are significantly longer than the Bragg wavelength [4], [5]. Passive radiometry at comparable wavelengths has been modeled using a similar description of the effect of the unresolved tilting of the surface by waves which are significantly longer than the radiation wavelength, but using the specular Fresnel relations to describe emission and scattering from the associated tilted facets [6], [7]. This level of modeling fails to account for the resonant effects of the small-scale surface roughness. Wu and Fung [8] and Wentz [9] extended the modeling to include resonant effects for isotropic surface roughness. Irisov *et al.* [10] further extended the modeling to include the effects of anisotropic wind-roughened surfaces on the directional dependence of polarimetric observations. Similar modeling by Yueh *et al.* [11]–[13] and Yueh [1] has been applied to the description of the variation of microwave brightness temperature with wind direction. The final Yueh modeling includes a description of the windward/leeward asymmetry of the distribution of short waves on long waves which is similar to that used by Donelan and Pierson [14] in application to scatterometer measurements. Comparisons of the model predictions with circle-flight K- and Ka-band polarimetric radiometer measurements by Yueh *et al.* [15], [16] are shown in Yueh [1] and reproduced in the right-hand side (180° to 360°) of Fig. 1. This includes the measured Stokes vector (T_v, T_h, U, V) at three incidence angles (30°, 55°, and 65°) and two radiometer frequencies (19 and 37 GHz). Upwind corresponds to 0° azimuth. The agreement with the qualitative features of the measurements suggests that the model includes the dominant mechanisms responsible for the modulation of brightness temperature with wind direction. The particular method chosen by Yueh [1] to implement his model ties it rigidly to the the Durden and Vesecky model wind–wave spectrum chosen to represent both the short-scale and long-scale ocean roughness [17]. Tuning of the Yueh model constants is, therefore, linked in a complicated way to the many constants associated with the model wind–wave spectrum. One of the properties of the spectrum entering into the Yueh model is the slope variance of large-scale waves. In order to make the theoretical model best agree with the data, Yueh increased the power-spectral-density (PSD) scaling of the model spectrum (a_0) by a factor of two from that of Durden and Vesecky. This brought the variance closer into agreement with that from other model spectra [14], [18], [19], but it was then higher by about a factor of two than the measurements of Cox and Munk [20]. This method of adjusting the model spectrum has the unfortunate consequence of making the interpretation of the several different effects more obscure. For example, increasing a_0 by a factor of two has the unwanted effect of also increasing the well-accepted Pierson–Moskowitz description of the longwave portion of the spectrum by a factor of two. A method that perturbs the model spectrum by increasing only the high wavenumber domain (which contributes the major portion of the total slope variance) and leaves the Pierson–Moskowitz domain unchanged requires more flexibility in the model spectrum.

An alternate approach that retains the spirit of the Yueh model is to isolate those local and global properties of the wave spectrum that enter into the radiance model in a way that permits them to be represented by a discrete number of parameters. These parameters can then be evaluated by any number of familiar techniques to optimize the agreement with available data. Such an approach, introduced by Baum and Irisov [2] in a study of the related problem of the modulation of microwave radiance by oceanic internal waves, will be examined here in relation to the Yueh model. A nominal (unoptimized) evaluation of the Baum–Irisov model is shown on the left (0° to 180°) side of Fig. 1 for comparison with the Yueh model. The qualitative features are comparable, but the modulation of T_h with azimuth angle is smaller than both the data and the Yueh [1] predictions. This short communication will describe the features of the model that simplify the process of optimizing the agreement with data.

II. Model

The Baum–Irisov model recognizes that a two-scale problem requires a spectral description of the rough ocean surface for wavenumbers close to that of the radiation to describe resonant (short-scale) effects. A parametric representation of this local spectral description is $G(K,\phi) = \mathrm{f}(\phi)g(k)(K/k)^{-\mathrm{n}}$, obtained from the PSD of the scalar wave height spectrum $g(K)$ evaluated at the radiation wavenumber k, along with a local spectral slope n. The directionality of the short waves

Manuscript received August 15, 2002; revised May 31, 2003. This work was carried out under Northrup Grumman Space Technology's Integrated Weather Products Testbed EVEREST facility.

The authors are with Northrop Grumman Space Technology, Redondo Beach, CA 90278 USA (e-mail: bruce.hauss@ngc.com).

Digital Object Identifier 10.1109/TGRS.2003.815970